Geochemistry, Geophysics, Geosystems

RESEARCH ARTICLE
10.1029/2019GC008529

Mapping Stress and Structure From Subducting Slab to Magmatic Rift: Crustal Seismic Anisotropy of the North Island, New Zealand

Finnigan Illsley-Kemp[1], Martha K. Savage[1], Colin J. N. Wilson[1], and Stephen Bannister[2]

[1]School of Geography, Environment and Earth Sciences, Victoria University of Wellington, Wellington, New Zealand, [2]GNS Science, Lower Hutt, New Zealand

Key Points:
- Results suggest the presence of large upper-crustal magma reservoirs at Taupō and Okataina, but not elsewhere in the rhyolitic central TVZ
- Stress in the northern Hikurangi forearc differs from the underlying slab, whereas stress in the southern subduction system is continuous
- The subducting Hikurangi slab is permeated by slab-bending related structures with possible relics from past subduction configurations

Supporting Information:
- Supporting Information S1
- Data Set S1
- Data Set S2
- Data Set S3
- Data Set S4

Correspondence to:
F. Illsley-Kemp,
finnigan.illsleykemp@vuw.ac.nz

Citation:
Illsley-Kemp, F., Savage, M. K., Wilson, C. J. N., & Bannister, S. (2019). Mapping stress and structure from subducting slab to magmatic rift: crustal seismic anisotropy of the North Island, New Zealand. *Geochemistry, Geophysics, Geosystems*, *20*. https://doi.org/10.1029/2019GC008529

Received 27 JUN 2019
Accepted 30 SEP 2019
Accepted article online 15 OCT 2019

Abstract We use crustal seismic anisotropy measurements in the North Island, New Zealand, to examine structures and stress within the Taupō Volcanic Zone, the Taranaki Volcanic Lineament, the subducting Hikurangi slab, and the Hikurangi forearc. Results in the Taranaki region are consistent with NW-SE oriented extension yet suggest that the Taranaki volcanic lineament may be controlled by a deep-rooted, inherited crustal structure. In the central Taupō Volcanic Zone anisotropy fast orientations are predominantly controlled by continental rifting. However at Taupō and Okataina volcanoes, fast orientations are highly variable and radial to the calderas suggesting the influence of magma reservoirs in the seismogenic crust (≤15 km depth). The subducting Hikurangi slab has a predominant trench-parallel fast orientation, reflecting the pervasive presence of plate-bending faults, yet changing orientations at depths ≥120 km beneath the central North Island may be relics from previous subduction configurations. Finally, results from the southern Hikurangi forearc show that the orientation of stresses there is consistent with those in the underlying subducting slab. In contrast, the northern Hikurangi forearc is pervasively fractured and is undergoing E-W compression, oblique to the stress field in the subducting slab. The north-south variation in fore-arc stress is likely related to differing subduction-interface coupling. Across the varying tectonic regimes of the North Island our study highlights that large-scale tectonic forces tend to dictate the orientation of stress and structures within the crust, although more localized features (plate coupling, magma reservoirs, and inherited crustal structures) can strongly influence surface magmatism and the crustal stress field.

1. Introduction

1.1. Tectonic Setting

The North Island of New Zealand is situated in a complex tectonic setting, largely controlled by the changing dynamics of the Pacific-Australian plate boundary over the past ~25 Myr (Figure 1). Through studying the seismic anisotropy in both the Pacific and Australian crust we can understand the orientation of the stress field and major crustal structures. In this study we utilize data from the GeoNet seismic network (Petersen et al., 2011), coupled with data from several temporary seismic deployments (Bannister, 2009; Ebinger, 2017; Reyners & Stuart, 2002), in order to create the largest catalog of crustal seismic anisotropy measurements in the North Island to date. This data set is used here to map the orientation and magnitude of crustal stresses beneath the volcanically active Taupō Volcanic Zone (TVZ) and Taranaki regions, the complex Hikurangi subduction zone forearc, and within the subducting Pacific plate itself.

The dynamic form (shape, vertical elevation, deformation patterns, faulting, and volcanism) of New Zealand's North Island is closely linked to the westward subduction of the Pacific plate beneath the Australian plate. The island is positioned between ocean-ocean subduction in the Tonga-Kermadec subduction system to the north and continental transpression in the South Island (Figure 1). The portion of the Pacific plate which is subducting beneath the North Island is the Hikurangi Plateau, an Early Cretaceous (120 Ma) oceanic plateau, thought to have formed as part of the Ontong Java Plateau (Mortimer & Parkinson, 1996; Taylor, 2006). Geophysical imaging of the Hikurangi Plateau through gravitational modeling and active source seismic imaging has revealed it to consist of 10–15 km thick crust (Davy & Wood, 1994; Wood & Davy, 1994; Tozer et al., 2017), although it has also been proposed that the crust is in fact up to 35 km thick

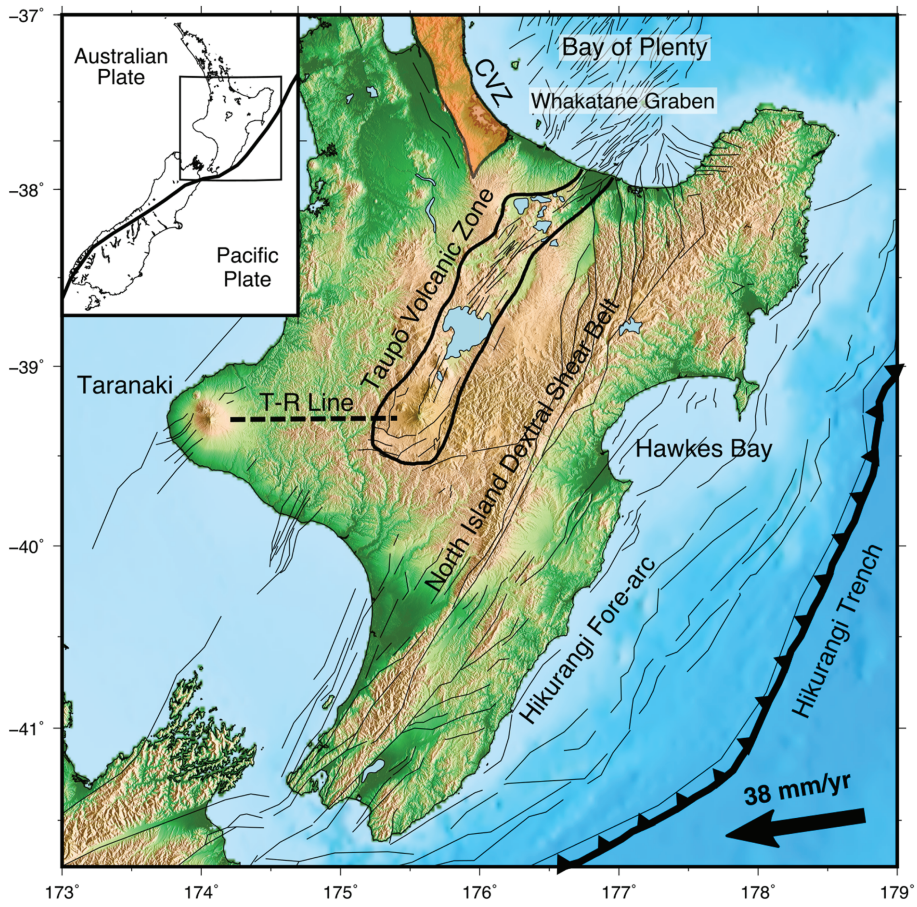

Figure 1. Selected geological features of the North Island of New Zealand. Thin black lines denote major mapped surface faults. CVZ = Coromandel volcanic zone. T-R Line = Taranaki-Ruapehu line. Outline for the young (≤350 ka) Taupō Volcanic Zone after Wilson et al. (1995) and Villamor and Berryman (2006a). Arrow shows the velocity of the Pacific plate relative to the Australian plate (DeMets et al., 2010).

(Reyners et al., 2011). The Hikurangi subduction zone has existed for approximately 23 Ma, but the trench has changed orientation during this time (King, 2000; Seebeck, Nicol, Giba, et al., 2014; Schellart et al., 2006; Seebeck, Nicol, Villamor, et al., 2014) and is currently characterized by westward, oblique subduction of the Pacific plate at a southwards decreasing rate of 5–6 to 2–3 cm/yr (Wallace et al., 2004). The Hikurangi subduction zone is thought to be capable of producing large (≥7 M_w) earthquakes, particularly in the south (Smith et al., 1989; Reyners, 1998), where currently the plate interface is largely locked. In contrast, the northern part of the subduction zone has been documented in recent years as hosting slow-slip events with moment releases of M_w=6.3–6.8 and recurrence intervals of 18–24 months (Shaddox & Schwartz, 2019; Wallace et al., 2012). This north-south contrast in megascopic slip behavior is attributed to a change in the coupling coefficient of the plate interface from coupled in the south to uncoupled in the north (Wallace et al., 2004).

In the eastern North Island, the oblique component of subduction of the Hikurangi Plateau is accommodated through dextral shear in the North Island dextral shear belt. Faults within the North Island dextral shear belt are predominantly westward dipping thrust faults with a lesser component of right-lateral strike-slip deformation (Nicol et al., 2007) and are capable of hosting large (≤8 M_w) earthquakes (Little et al., 2010; Rodgers & Little, 2006; Van Dissen & Berryman, 1996). To the northwest of the North Island dextral shear belt lies the volcanically active Taupō Volcanic Zone. The TVZ has been volcanically active for approximately 2 Ma, and since 1.85 Ma it has been dominated by rhyolite volcanism (Chambefort et al., 2014; Eastwood et al., 2013). Wilson et al. (1995) divide the TVZ into three distinct sections along its length. The southern and northern TVZ sectors are typical of subduction-related arcs worldwide, with dominantly andesitic volcanism building large composite volcanoes such as Ruapehu, Tongariro, and White Island (Whakaari). In contrast

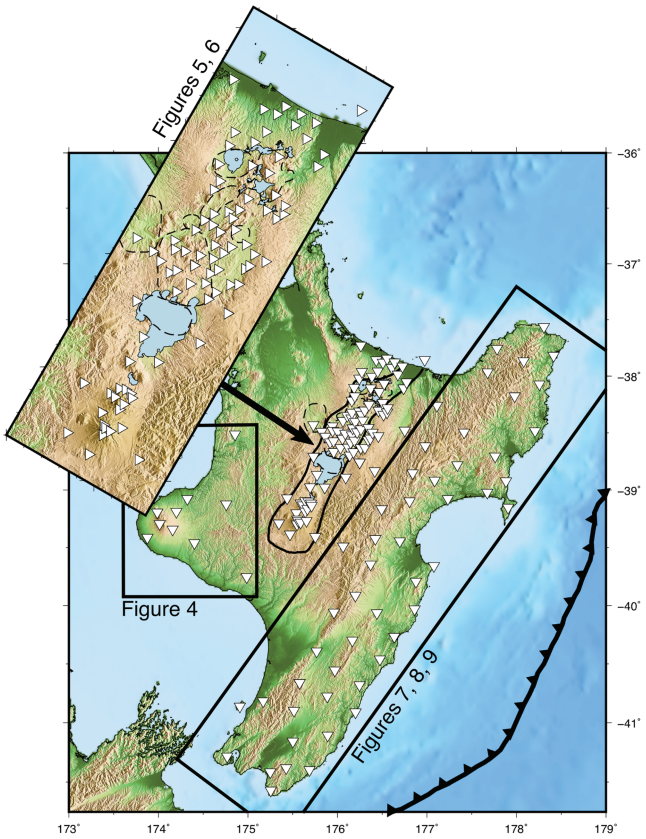

Figure 2. The seismic stations used in our study to calculate seismic anisotropy from local earthquakes. This combined seismic network of 156 stations comprises the permanent GeoNet network (Petersen et al., 2011), plus stations from the central North Island passive seismic experiment (Reyners & Stuart, 2002), Hotter and Deeper (Bannister, 2009), and back-arc rifting in New Zealand deployments (Ebinger, 2017). The inset shows the Taupō Volcanic Zone, where our station density is highest.

the central TVZ is characterized by anomalously high surface heat flow (Bibby et al., 1995) and exceptionally voluminous rhyolite volcanism (Wilson et al., 2009), particularly over the last 50–60 kyr at Taupō and Okataina volcanoes. The TVZ is the southernmost extension of the Tonga-Kermadec arc and also hosts the Taupō continental rift, with extension induced by the oblique subduction of the Pacific plate (Cole, 1990). Present-day rates of extension across the TVZ increase from ≤5 mm/yr at Ruapehu, to 13–19 mm/yr at the Bay of Plenty coastline and increasing into the offshore Whakatane graben (Lamarche et al., 2006; Wallace et al., 2004). The orientation of extension, relative to the rift, varies from orthogonal in the south to oblique in the north (Seebeck, Nicol, Villamor, et al., 2014).

Running east-west between Ruapehu and Taranaki volcanoes lies the crustal feature known as the Taranaki-Ruapehu Line. This line marks the boundary between 25-km thick crust to the north and ~32-km thick crust to the south, over a transition which is interpreted to represent an abrupt step in the Moho (Dimech et al., 2017; Salmon et al., 2011). It has been proposed that the Taranaki-Ruapehu Line is a result of delamination of the lower crust and mantle lithosphere to the north (Dimech et al., 2017; Stern et al., 2013). At the western end of the Taranaki-Ruapehu Line lies Taranaki (Figure 1), an andesitic volcano which last erupted in ~1755 AD (Druce, 1966). Taranaki is the youngest of four andesite volcanoes which form a linear chain, known as the Taranaki lineament, oriented NNW-SSE (Price et al., 1999; Zernack et al., 2011). Taranaki volcano lies at the southern end of the offshore Taranaki basin, in which andesite volcanism has migrated from north to south over the last ~16 Ma (Giba et al., 2010). The Taranaki basin is characterized by NE-SW oriented normal faulting, thought to be induced by back-arc rifting, and the region is further complicated by a complex tectonic history including the Taranaki fault, a subduction back thrust (Stagpoole & Nicol, 2008). The exact origin for volcanism at Taranaki is not clear as it lies ~180 km west of the TVZ;

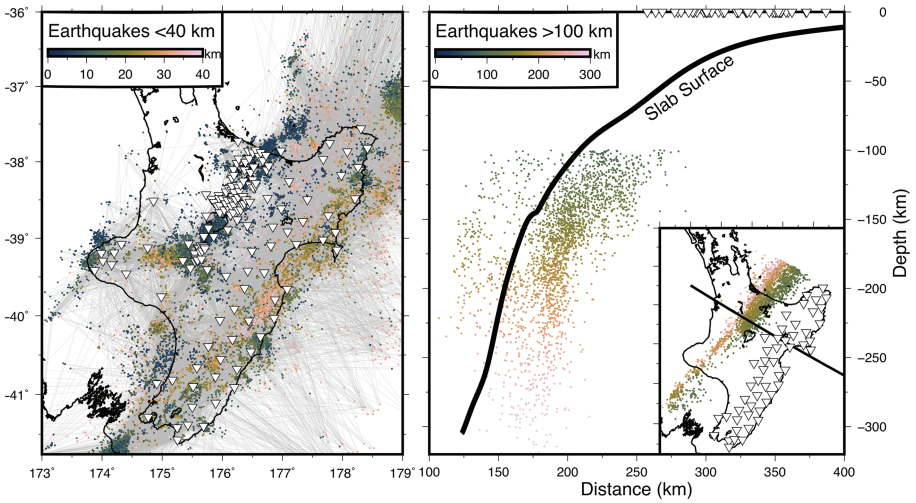

Figure 3. All of the earthquakes that yielded high-quality seismic anisotropy measurements. The left panel shows earthquake locations and raypaths for all events that occurred at ≤40 km depth. These measurements are used to interpret seismic anisotropy in the Australian plate and Hikurangi forearc. The right panel shows a cross section through the mantle below the North Island with all events with depths greater than 100 km projected onto a vertical plane aligned along the black line in the inset panel. These measurements are used to interpret seismic anisotropy in the subducting Hikurangi slab. The black line in the main panel denotes the top surface of the subducting Hikurangi slab (Williams et al., 2013).

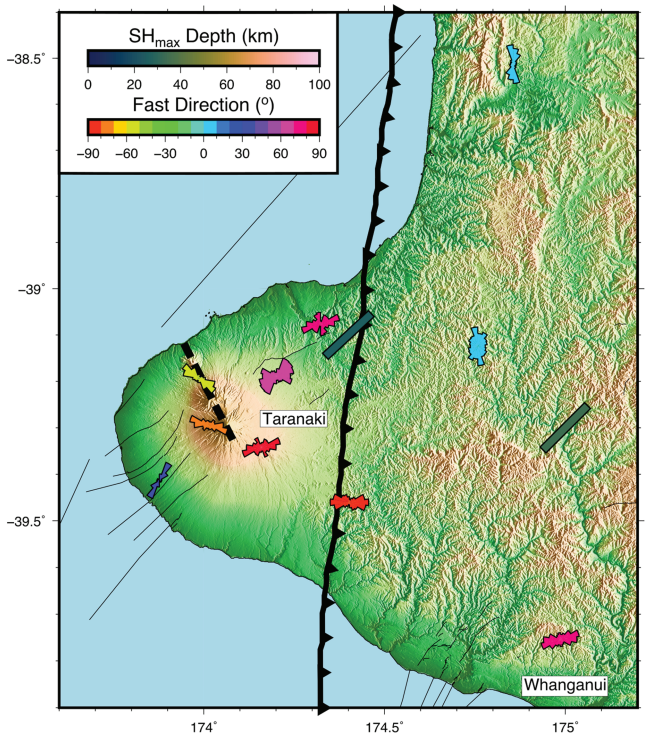

Figure 4. Results from the Taranaki region. Seismic fast orientation results at individual seismic stations plotted as rose diagrams (circular histograms). If the standard error of fast orientations at an individual station is less than 10°, then the rose diagram is colored by the mean orientation, otherwise it is gray. Colored bars show SH_{max} orientations calculated from focal mechanisms, revealing the orientation of the stress field at specific depths (Townend et al., 2012). Thick dashed line denotes the Taranaki lineament. The surface projection of the trace of the eastward-dipping Taranaki reverse fault is shown by the thick black line (Stagpoole & Nicol, 2008). Thin black lines denote active faults (http://data.gns.cri.nz/af/).

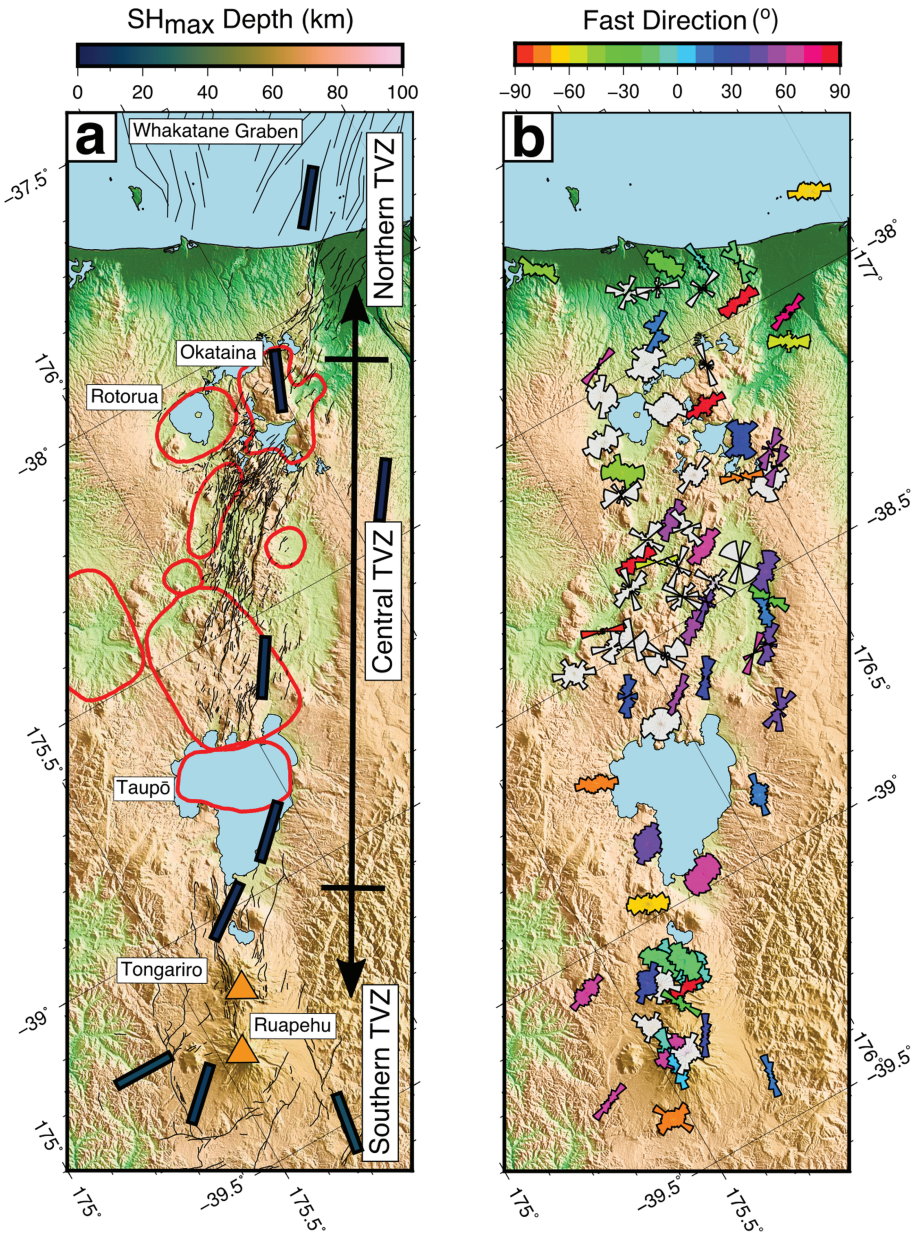

Figure 5. (a) Geological features of the TVZ. Black lines denote active faults from the New Zealand active fault database (http://data.gns.cri.nz/af/); red outlines denote rhyolite calderas (Wilson et al., 2009); and orange triangles denote andesite volcanic centers Tongariro and Ruapehu. Colored bars show SH_{max} orientations calculated from focal mechanisms, revealing the orientation of the stress field at specific depths (Townend et al., 2012). (b) Fast orientation results at individual seismic stations plotted as rose diagrams (circular histograms). If the standard error of fast orientations at an individual station is less than 10° then the rose diagram is colored by the mean direction, otherwise it is gray. TVZ = Taupō Volcanic Zone.

therefore, Stern et al. (2013) have proposed that lithospheric delamination drives the production of mantle melts.

1.2. Seismic Anisotropy in the Crust

Seismic anisotropy, the directional dependence of seismic wave speed, is an intrinsic property of the Earth's crust and can be measured by the detection of shear-wave splitting (Illsley-Kemp et al., 2017; Johnson et al., 2011; Li & Peng, 2017; Savage, 1999). Numerous studies have suggested that seismic anisotropy is caused by structural features such as faults (Boness & Zoback, 2006; Zinke & Zoback, 2000) and/or aligned melt pockets (Ando & Ishikawa, 1982; Bastow et al., 2010; Dunn et al., 2005; Keir et al., 2011), where the shear-wave fast

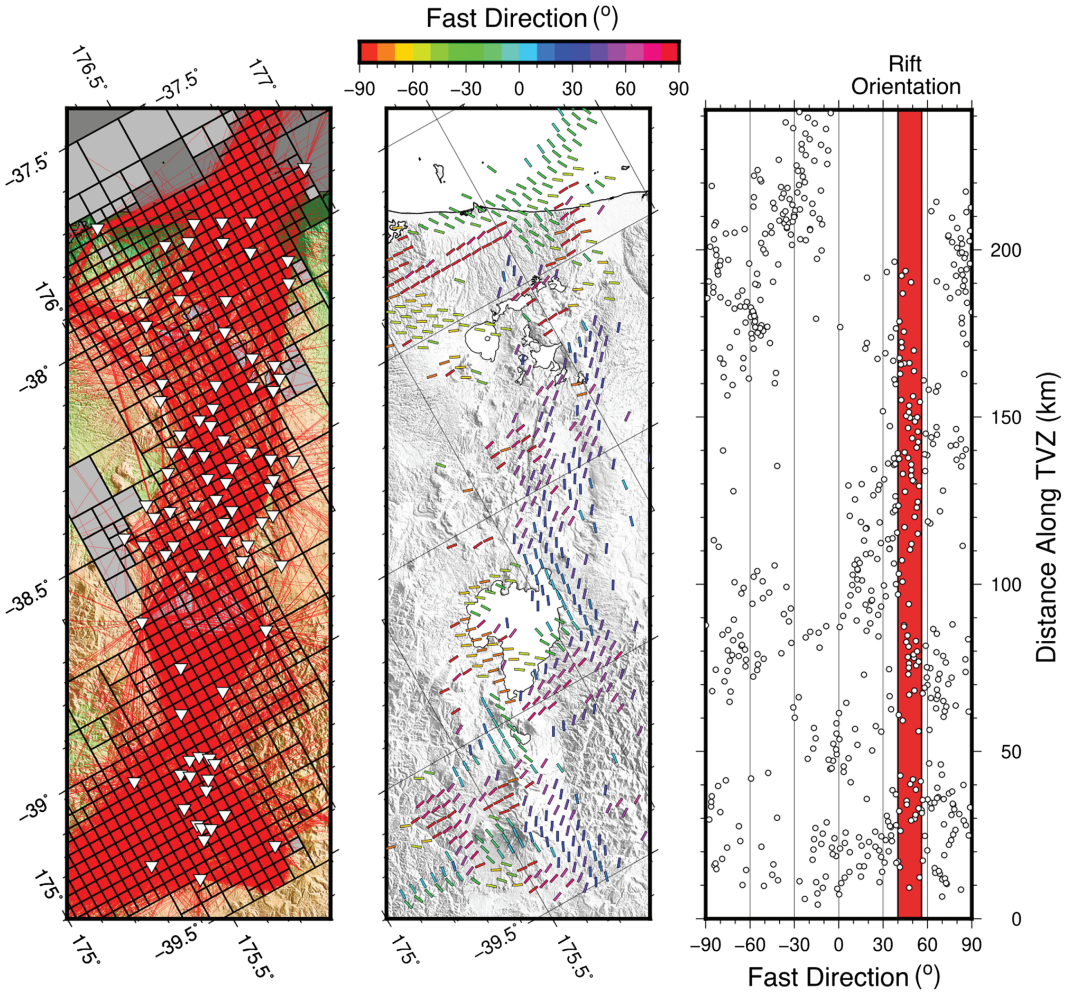

Figure 6. Spatial averaging of fast orientations throughout the TVZ. (a) Ray-path coverage and gridding distribution. Gray boxes denote regions that were not resolved. White triangles are seismic stations; red lines are straight raypaths between earthquake and station. (b) Well-resolved fast orientations across the TVZ, colored for orientation. (c) Projection of fast orientations along the TVZ. The red region shows the approximate orientation of the Taupo rift (40–55°). TVZ = Taupō Volcanic Zone.

orientation is parallel to the trend of structural features. It has also been increasingly inferred that seismic anisotropy in the crust can be controlled by aligned, fluid-filled microcracks (Crampin & Peacock, 2008, and references therein). Microcracks exist between grains and can be assumed to have a simple, penny-shaped geometry (Crampin, 1994, 1999; Hudson, 1981). It is thought that these microcracks are randomly oriented in the crust and do not intrinsically induce seismic anisotropy. However, when a horizontal stress is applied to the crust, microcracks that are aligned with the direction of maximum (σ_1) horizontal compressive stress will selectively open, and those perpendicular to σ_1 will close. These open, aligned, fluid-filled microcracks will then induce seismic anisotropy through a mechanism described as extensive dilatancy anisotropy, such that the fast orientation is parallel to the maximum horizontal compression (SH_{max}) (Crampin, 1984, 1987). The variation in orientations of individual, open microcracks can vary by ~30°–40° (Crampin & Zatsepin, 1997). However, because the wavelengths of seismic waves are much longer than the dimensions of the microcracks, the average crack orientation is effectively sampled. The magnitude of seismic anisotropy (i.e., the delay time between shear waves) has been shown to be controlled by the aspect ratio (ratio between width and length) of the microcracks (Crampin, 1999). The microcrack's aspect ratio correlates with the horizontal stress; hence, the magnitude of seismic anisotropy can be directly related to the magnitude of maximum horizontal stress. Therefore, seismic anisotropy can be used to directly measure the orientation and magnitude of the horizontal stress field throughout the sampled volume of crust in the areas of interest.

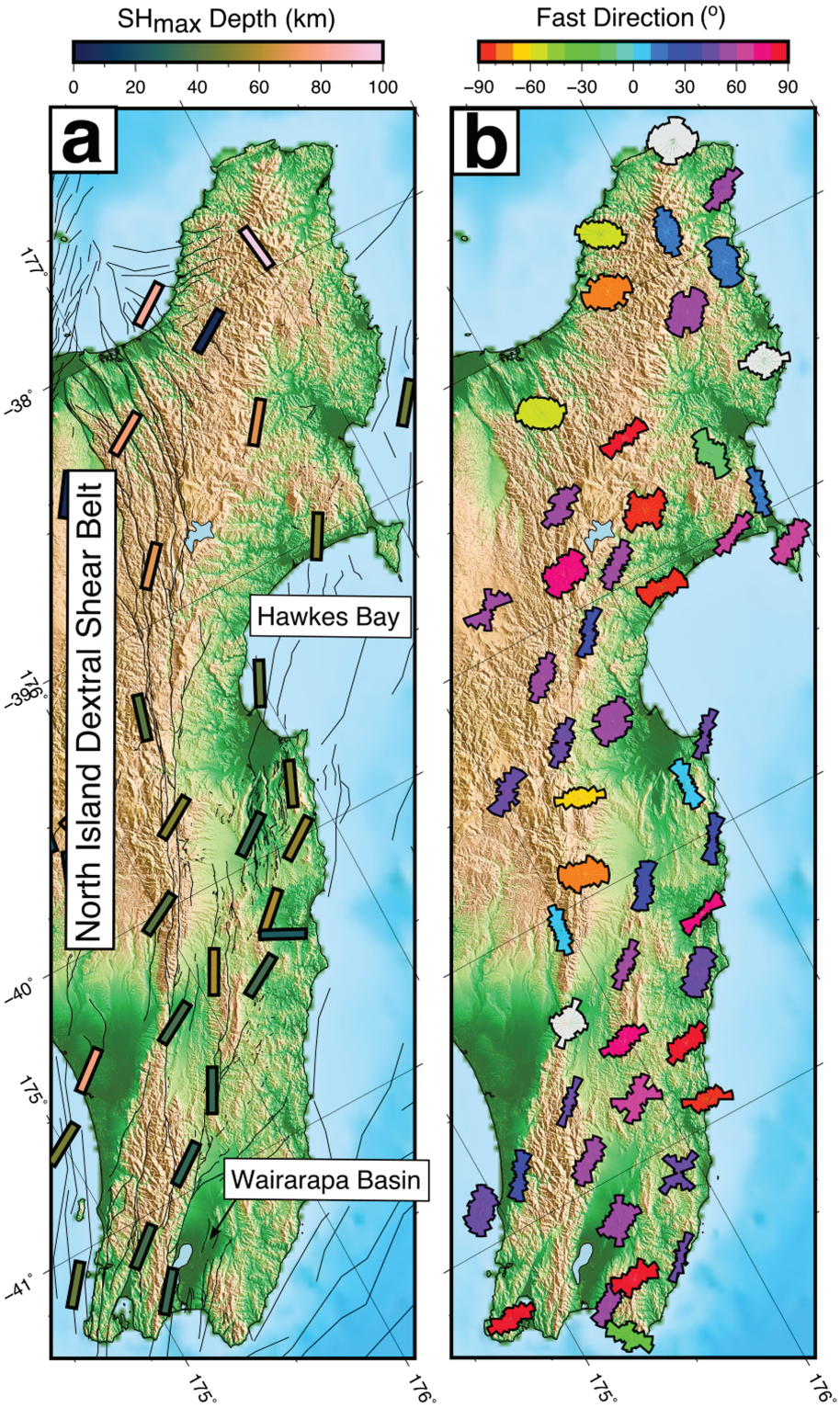

Figure 7. (a) Geological features of the Hikurangi fore-arc region. The North Island dextral shear belt accommodates the oblique subduction of the Hikurangi plate (Nicol et al., 2007). Colored bars show SH_{max} orientations calculated from focal mechanisms, revealing the orientation of the stress field at specific depths (Townend et al., 2012). Black lines denote active surface faults (http://data.gns.cri.nz/af/). (b) Fast orientation results at individual seismic stations plotted as rose diagrams (circular histograms). If the standard error of fast orientations at an individual station is less than 10° then the rose diagram is colored by the mean orientation, otherwise it is gray.

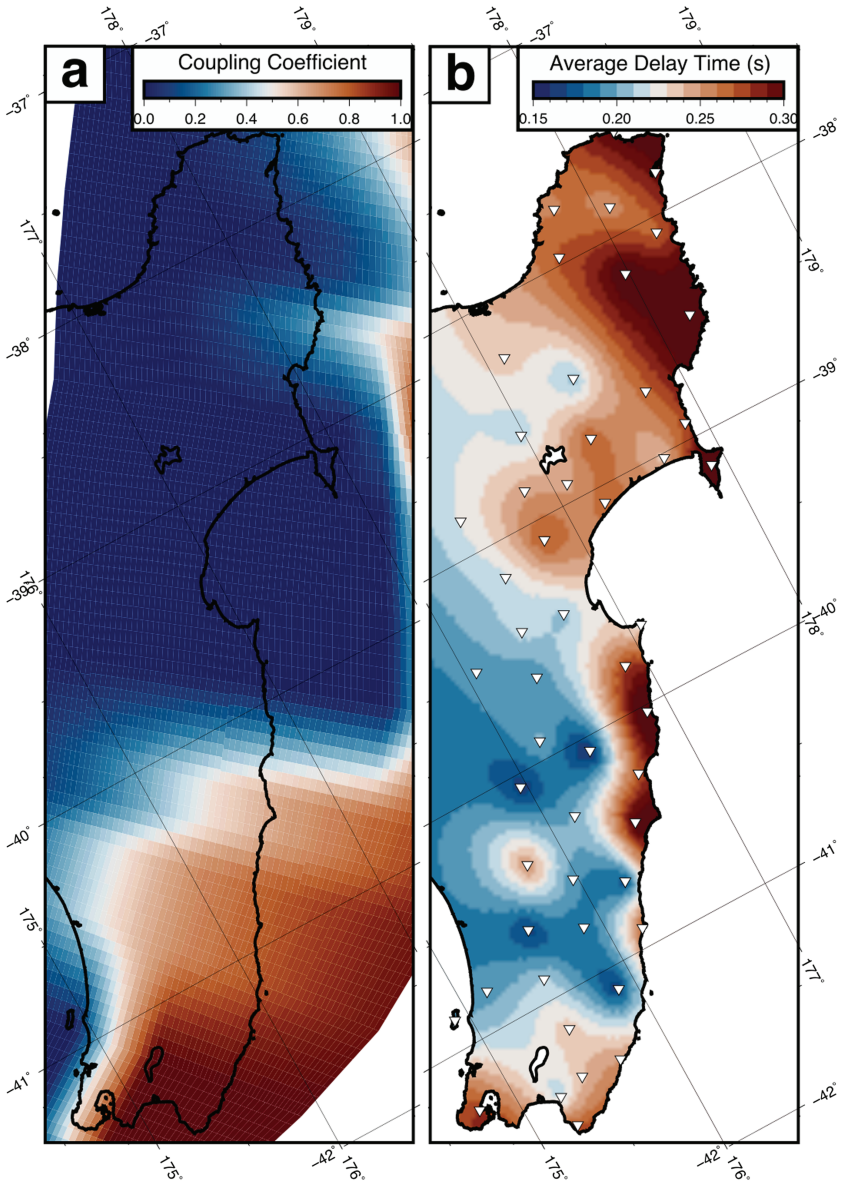

Figure 8. (a) Surface of the coupling coefficient of the subduction zone interface (Wallace et al., 2004). (b) Surface of the average shear-wave splitting delay time (seconds) at each station.

2. Data Sources & Method

Our catalog of seismic anisotropy measurements is compiled by combining several seismic data sets (Figure 2). The largest is from the GeoNet seismic network from which we collate all earthquakes which have manually picked S-wave arrivals and available waveforms up to July 2018 (Petersen et al., 2011). This data set is then supplemented by manually picked S-wave arrival times from three temporary seismic deployments; the central North Island passive seismic experiment (Reyners & Stuart, 2002), the Hotter and Deeper array (Bannister, 2009), and the back-arc rifting in New Zealand array (Ebinger, 2017). We then applied the Multiple Filter Automatic Splitting Technique (MFAST) (Savage et al., 2010) on all of the associated waveforms. MFAST develops upon previous work (Silver & Chan, 1991; Teanby et al., 2004) to measure seismic anisotropy by finding the minimum of the smallest eigenvalue of the horizontal particle motion by performing a grid search over a range of fast orientation (-90° – 90°) and delay times (0–0.8 s). It then performs a rigorous cluster analysis which provides an estimate of the "quality" of each measurement. By applying this technique to our compiled data we produce a total of 96,350 high-quality (signal-to-noise ratio $\geq$3, fast orientation standard error $\leq$ 25°, and incidence angle $\leq$ 35°) measurements of seismic anisotropy at 156

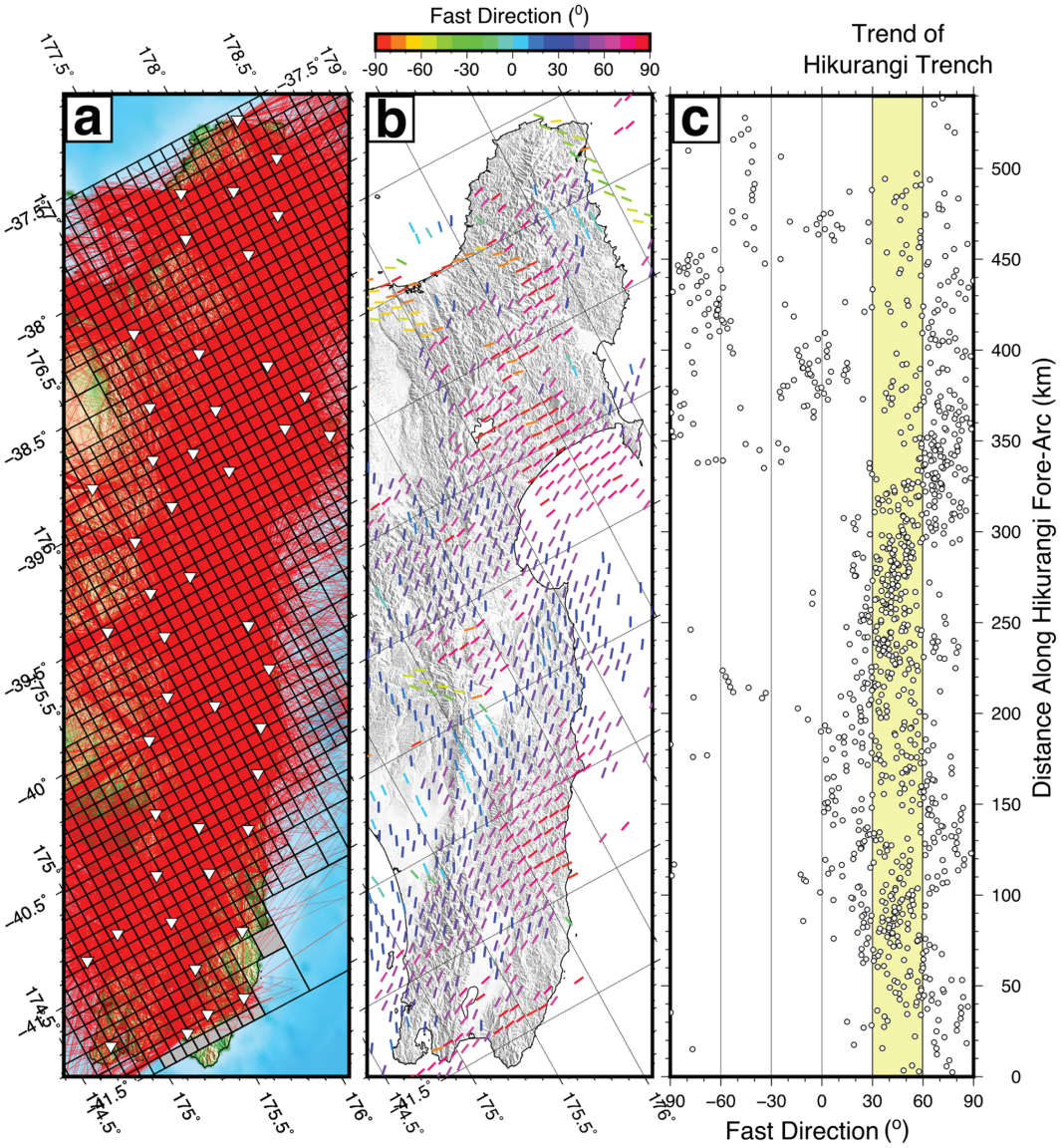

Figure 9. Spatial averaging of fast orientation throughout the Hikurangi forearc. (a) Raypath coverage and gridding distribution. White triangles are seismic stations, and red lines are straight raypaths between earthquake and station. (b) Well-resolved fast orientations across the Hikurangi forearc, colored for orientation. (c) Projection of fast orientations along the forearc. The yellow region shows the approximate trend of the Hikurangi trench.

seismic stations (Figure 3). At each station we calculate the mean fast orientation by adding unit vectors, given by the measured fast orientation, and dividing by the number of measurements (Savage et al., 2010). This also requires consideration of the 180° ambiguity in orientation. The length of the resultant vector gives an indication of the standard error, which we consider when interpreting our results.

Such a large volume of shear-wave splitting measurements can be difficult to interpret and often exhibit an azimuthal dependency in anisotropy measurements. To gain insight into the spatial distribution of anisotropy orientations we use the 2-D splitting tomography code (TESSA) of Johnson et al. (2011). This computes average fast orientations in 2-D grids using circular statistics, but does not take depth variations into account. We plot results from grids that feature at least 10 crossing rays and have a standard deviation in fast orientation of less than 30° and standard mean error of less than 10° .

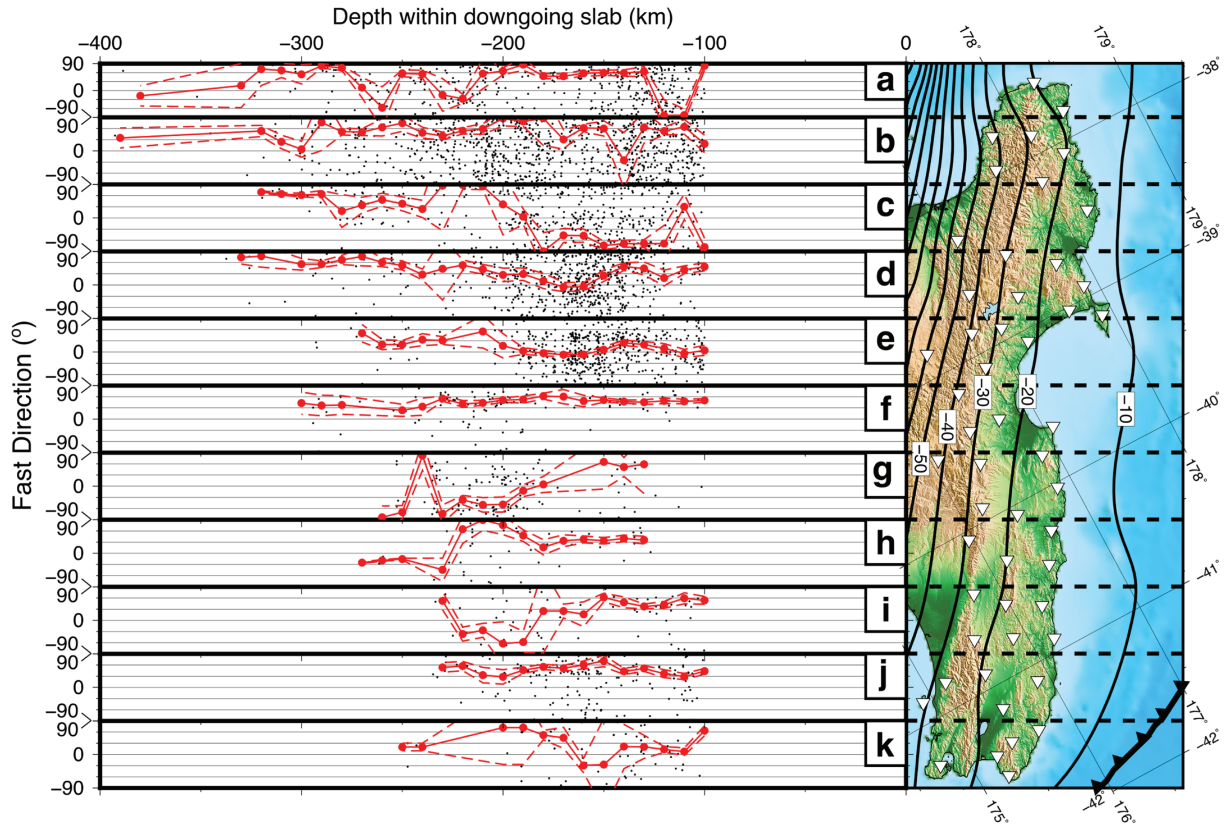

Figure 10. Seismic anisotropy fast orientations in the subducting Hikurangi slab. The slab is divided into 11 cross-sections and anisotropy measurements with a subduction-parallel raypath are plotted as a function of orientation (°) and depth (km). Individual measurements are plotted as black points. Mean fast orientation is calculated at 10 km intervals and plotted as red circles and ±standard error is plotted as dashed red line. Contours of depth to the top surface of the slab are plotted in map view (Williams et al., 2013).

3. Results

Here we consider our results within four separate geographical/geological regions, each of which have distinct volcanic and/or tectonic characteristics.

3.1. Taranaki Region

In the Taranaki region we have measured 2,622 high-quality seismic anisotropy measurements across 10 seismic stations, spanning data from 2005 to July 2018 (Figure 4). We observe a large amount of variation in average station orientations. On the western and northwestern flanks of Taranaki volcano the fast orientation is oriented NW-SE, aligned with the Taranaki lineament. In contrast, to the southeast and northeast of Taranaki, the fast orientation is oriented NE-SW. Further to the northeast of the Taranaki region, the fast orientation is N-S, and in the Whanganui region is ENE-WSW.

3.2. Taupō Volcanic Zone

In the TVZ we have derived 42,644 high-quality measurements of seismic anisotropy, distributed across 99 seismic stations, with data spanning the period from 2001 to May 2019. Many of the individual stations show self-consistent fast orientations, with standard errors of $\leq 10°$ (Figure 5). However, there is a large amount of variation in average fast orientation throughout the TVZ, and several stations show a bimodal distribution of fast orientations which is not captured by a simple standard error. The earthquake-receiver distribution of our combined network provides excellent ray coverage for spatial averaging of fast orientations. For the splitting tomography we constrain the minimum grid size to be 3×3 km, and each box must have a minimum of 10 crossing rays (Johnson et al., 2011). This enables us to retrieve well-constrained, low-variability estimates of fast orientations throughout the entire TVZ (Figure 6). In order to better examine how fast orientations change in the TVZ, we also plot the fast orientation as a function of distance along the TVZ axis (Figure 6c).

The most notable feature of our results is the consistency of the fast orientation in the central TVZ, between Taupō and Okataina (100–180 km along projection, Figure 6c). The fast orientation here is between 30° and 60° , with relatively little variability. In contrast at either end of this region, at Taupō and Okataina, the fast orientation shows no predominant trend and has a large amount of variation. At Okataina, the rift-aligned anisotropy in the central TVZ appears to intersect with a region of NW-SE fast orientations which extend through Rotorua caldera. In addition, there are several measurements of E-W fast orientations within the Okataina caldera. The fast orientations around Taupō caldera vary greatly. Many measurements are radial to the caldera, particularly those close to the caldera rim. However, this radial pattern does not persist further outside the caldera, in particular fast orientations to the south and southeast of the caldera are ∼E-W and rotate to a N-S orientation to the east of the caldera.

In the southern TVZ, the distribution of fast orientations is highly complex. Between Tongariro volcano and the southern end of Lake Taupō, the fast orientation is consistently N-S. However, this alters dramatically at Tongariro volcano where the fast orientation is E-W, a pattern which extends to the west. At Ruapehu volcano, the fast orientation is N-S to NE-SW, but this again changes to E-W south of Ruapehu. To the east of the volcanoes, the fast orientation is ∼NE-SW. In the northern TVZ the fast orientations are dominated by two orientations, E-W and NNW-SSE (∼-30°). The NNW-SSE orientation is predominantly located at the coastline and in the offshore Whakatane graben, whereas, the E-W fast orientation is located to the west of the northern TVZ.

3.3. Hikurangi Fore-Arc

In the Hikurangi fore-arc region we make 45,349 high-quality measurements across 53 seismic stations, with data spanning 2005 to July 2018. Average fast orientations at individual stations show low variation, with all but three stations showing a consistent average fast orientation (Figure 7b). Across the region, there is a fairly consistent NE-SW fast orientation. We also calculate the average shear-wave splitting delay time (seconds), which gives an indication of the magnitude of seismic anisotropy. We observe that there is a tendency for delay time to increase towards the Hikurangi margin (Figure 8b). The distribution of earthquakes and seismometers provides almost complete ray coverage in the fore-arc regions for the splitting tomography. We constrain the minimum grid size to be 6×6 km (Figure 9a) and again plot fast orientation as a function of distance along the Hikurangi forearc.

The fast orientation in the Hikurangi forearc is dominated by a NE-SW, trench-parallel orientation (30°−60°) (Figure 9b). This orientation is particularly characteristic of the region extending from the Wairarapa basin to central Hawkes Bay. In the northeastern forearc, the NE-SW fast orientation is not so prevalent, and the region is characterized by a ENE-WSW (60°−90°) fast orientation, but with larger amounts of variation. A significant departure from a trench-parallel fast orientation is observed ∼200 km along the North Island dextral shear belt, where the fast orientation is NW-SE (–60°−−30°) (Figures 7b and 9b).

3.4. Subducting Hikurangi Slab

In order to investigate variations in seismic anisotropy in the subducting Hikurangi slab we selected earthquakes that had a station–earthquake raypath that was approximately parallel to the dip of the subducting slab (∼300°). By doing this, the anisotropy measurements will originate from earthquake raypaths that sample large portions of the downgoing slab, as the fast internal velocities of the slab will act as a waveguide (Eakin et al., 2016). We confirm this behavior by comparing the S-wave frequencies of these deep earthquakes at stations in the Hikurangi arc and in the NW of the North Island (Supporting information Figure S1). We then produce multiple "cross-sections" of slab anisotropy along the length of the subduction zone (Figure 10), to produce a database that consists of 5,735 high-quality seismic anisotropy measurements. The depth extent of our measurements increases from ∼250 km in the south of the subduction zone, to ∼400 km in the north. This pattern of northward increasing earthquake depth generally reflects the earthquake activity (Eberhart-Phillips et al., 2013). We then calculate average fast orientation using circular statistics (Savage et al., 2010) over 20 km "bin" widths at 10 km intervals (red circles in Figure 10). For each of these bins we calculate the standard error in mean and plot this as an upper and lower error bar (dashed red line in Figure 10).

Seismic fast orientation within the downgoing slab varies both with depth and with distance along the Hikurangi margin (Figure 10). Profile a, in the northern Hikurangi margin, shows a predominant NE-SW fast orientation (30° − 60°) but with deviations to a NNW-SSE orientation at depth of 220–230 and 260–270 km. Profile b has a predominant NE-SW orientation at all depths. Profile c shows a sharp change from depths

of 100–190 km, where fast orientations are ENE-WSW before changing to a NE-SW orientation at depths ≥200 km. Profile d shows a smaller amount of variation, with the majority of fast orientations being NE-SW, however there is a deviation to a N-S orientation at 160–170 km. Profile e shows fairly consistent N-S fast orientations throughout the slab and profile f shows an equally consistent NE-SW orientation. Profiles g–k generally have fewer measurements of anisotropy, so errors in the calculation of mean fast orientation tend to be larger; however, profiles i and k also show consistent NE-SW fast orientation throughout the slab.

4. Discussion

4.1. Taranaki Region

Much of the anisotropy in the Taranaki region has a NE-SW fast orientation, which is aligned with previous estimations of SH_{max} (Sherburn & White, 2006; Townend et al., 2012) as well as mapped faults (Figure 4). These observations suggest that the region is undergoing a similar, though not as rapid, NW-SE oriented extension as that observed in the TVZ, and that this is controlling the anisotropy. Approximately, 30% of the earthquakes which yield anisotropy measurements occur in the lower-crust/upper-mantle (≥20 km depth). At these depths we may expect to observe seismic anisotropy that is influenced by the proposed mantle delamination (Dimech et al., 2017); however, there is no discernible change in fast orientations with increasing depth. We therefore suggest that the NW-SE oriented extension observed in the upper crust also extends to lower-crustal depths, or that any shear-wave splitting from deep structures is masked by subsequent splitting at shallow levels.

Fast orientations to the northeast of Taranaki show N-S orientations, which may be influenced by structures associated with the N-S trending Taranaki Fault (Figure 4). However, fast orientations on the Taranaki volcanic edifice deviate significantly from this NE-SW orientation and are oriented NW-SE. Volcanism in the Taranaki region is confined to the NNW-SSE trending Taranaki lineament, and the locus of active volcanism here has generally migrated SE through time (Neall et al., 1986; Price et al., 1999). The underlying reason for this NNW-SSE trend has not been established. In extensional environments volcanic fields will typically follow trends that are perpendicular to the direction of extension (e.g., Mazzarini et al., 2016). Significant deviations from this require the influence of either local perturbations to the stress field or inherited crustal structures (Wadge et al., 2016). Proposed examples of volcanic lineaments which follow inherited crustal structures include the Nabro range, Ethiopia/Eritrea (Wiart & Oppenheimer, 2005), and the Jemez volcanic field, USA (Self et al., 1986). As noted previously, the mapped faults in the region strike NE-SW to N-S (Figure 4) and provide no evidence for recently active NNW-SSE oriented structures. It has been suggested the along-axis segmentation in the TVZ may be controlled by the presence of deep-rooted, cross-cutting NNW-SSE trending structures (Rowland & Sibson, 2001). Perhaps, similar basement structures are the underlying cause for the Taranaki lineation and it is these crustal structures that are inducing the NW-SE fast orientation that we observe. A more detailed geophysical investigation into the underlying cause for the Taranaki lineation could shed further light on the deeper roots of this volcanic system.

4.2. Taupō Volcanic Zone

In the central TVZ, between Taupō and Okataina, the fast orientation is aligned parallel to the rift (Figures 5b and 6b,c), in agreement with the previous study of Audoine et al. (2004). This alignment is parallel to the rift-related faults in this region (Figure 5a), and it could be that these aligned structures are inducing the NE-SW fast orientation (e.g., Li et al., 2014). However, the central TVZ also hosts many caldera structures that are not preferentially aligned with the rift (Figure 5a). We see no evidence that the seismic fast orientation is aligning with these caldera structures in the central TVZ; thus, we suggest that shallow, caldera-related crustal structures are not the dominant control on seismic anisotropy in this region. The orientation of extension in the TVZ (Seebeck et al., 2014; Villamor & Berryman, 2001; Wallace et al., 2012), along with earthquake focal mechanisms (Townend et al., 2012), suggests that the direction of maximum horizontal compression (SH_{max}) is oriented NE-SW, parallel to the fast orientation. We therefore propose that the anisotropy in the central TVZ is controlled by rift-related extensional stress and that this is dominant throughout the thickness of the seismogenic crust (~15 km), consistent with the conclusions of Townend et al. (2012). This observation has also been made on a smaller scale in the Rotokawa and Ngatamariki geothermal field (Mroczek et al., 2019). Major geothermal systems have been imaged by magnetotelluric surveys at ≤10-km depth in the central TVZ (Bertrand et al., 2012; Heise et al., 2010), yet the relevant crustal

resisitivity anomalies have no observable influence on anisotropy. This may mean that the geothermal systems are also heavily influenced by continental rifting and fluids occupy voids or fractures, that on the local scale of each system, are preferentially aligned along rift-related structures.

In contrast to the rift-aligned fast orientation in the middle portion of the central TVZ, we observe varied anisotropy patterns at its northern and southern limits around Taupō and Okataina volcanoes. In these regions the fast orientation is not oriented with the rift and does not show a clear, dominant orientation (Figure 6b,c). Both of these volcanoes have hosted the most recent (≤61 ka) large-volume rhyolite eruptions in the TVZ (Wilson et al., 2009) and host major caldera collapse structures with associated negative gravity anomalies (Davy & Caldwell, 1998; Seebeck et al., 2010). The formation of these calderas would be accompanied by similarly orientated collapse structures in the surrounding crust, and one may expect that these could control the anisotropy. However, this would result in fast orientations that are approximately arcuate around the two calderas. This is not what we observe, and we must invoke an alternative explanation. Petrological studies of recent (post-25 ka) eruptive products from Taupō suggest that a large (≥200 km^3) silicic magma reservoir (mush: dominantly crystals with subordinate amounts of melt) currently exists beneath the Taupō caldera at ~4–12 km depth (Barker et al., 2015; Liu et al., 2006). Similarly, petrological and magnetotelluric studies of Okataina caldera suggest a large, silicic mush magma reservoir also exists beneath Okataina at ~8–15 km depth (Cole et al., 2014; Heise et al., 2010). The presence of such large magma systems in these regions will cause a significant reduction in crustal viscosity and have been proposed to influence rifting in the TVZ (Ellis et al., 2014). It may be that large, silicic magma chambers beneath Okataina and Taupō alter the bulk crustal rheology such that the extensional stress-field cannot induce anisotropy through the preferential opening of microcracks. Alternatively, localized large stresses or changes in anisotropy within large magma chambers may be altering the observed anisotropy (Maher & Kendall, 2018). Many of the fast orientations on the margins of the Taupō caldera are oriented radially to the caldera (Figure 6b). This pattern of radial SH_{max} has been observed at several volcanoes worldwide and is thought to be caused by either inflating magma chambers (Illsley-Kemp et al., 2018; Savage et al., 2015) or gravitational loading (Araragi et al., 2015). Gravitational loading is not a viable explanation for the radial fast orientations at Taupō, as the caldera produces a negative gravity anomaly (Davy & Caldwell, 1998). If the magma reservoir beneath Taupō were inflating at the present day, it would induce ground deformation, which is not observed. However, ground deformation related to inflation may be obscured by the influence of caldera-bounding faults beneath Lake Taupō (Ellis et al., 2007). Future geophysical studies of the present state of the Taupō magmatic system will enable the detailed modeling of potential deformation-related stresses and associated anisotropy. Thus, our results provide further geophysical evidence to suggest that Taupō and Okataina currently host significant magma chambers. As we have shown that rift-induced seismic anisotropy is present throughout the seismogenic crust between Taupō and Okataina, we can extend our hypothesis further to suggest that middle to upper crustal magma reservoirs, of a similar scale to Taupō and Okataina, do not presently exist in this region. It may be that the high surface heat flow in this region (Bibby et al., 1995) is sourced from lower-crustal/mantle magma storage regions, as suggested by Stern and Benson (2011). Throughout the central TVZ we observe very little variation in fast orientation with time, suggesting that anisotropy has remained relatively constant for at least the previous decade. Seismic anisotropy has been proposed as a tool for detecting volcanic unrest (Gerst & Savage, 2004), whereby pressure changes in the magmatic system alter the observed fast orientation. The lack of time-varying anisotropy in the central TVZ therefore suggests that either the region has been in a period of magmatic quiescence for the last ~10 years or the resolution of our data is not sufficient to detect unrest.

In the southern segment of the TVZ, in the region of Tongariro and Ruapehu, the fast orientation is predominantly either N-S or E-W (Figure 6b), as also observed by Johnson et al. (2011) and Johnson and Savage (2012). These studies infer that the perpendicular orientations are both induced by stress-aligned microcracks. Extension rates related to the Taupō rift decrease southward and are minimal in the Ruapehu region (Wallace et al., 2004), and it is therefore not surprising that a rift-related fast orientation does not characterize this region. The southern TVZ hosts perpendicular N-S and E-W normal fault sets, and we suggest that these are parallel to the smaller-scale structural features controlling the observed perpendicular fast orientations (Figure 5a). (Villamor & Berryman, 2006a, 2006b) studied the surface expression of these faults in detail, but could not measure fault orientations at depth. We can use our anisotropy measurements to suggest the dominant fault orientation throughout the seismogenic crust in different areas. We therefore suggest that

E-W faulting dominates to the north, south, and west of Ruapehu, but that N-S faulting dominates beneath and to the east of the Ruapehu edifice during our study period.

In the northern segment of the TVZ, anisotropy in the Whakatane graben region needs to be interpreted with caution, as our data provide little variation in azimuth direction (Figure 6a). The fast orientation in this region is highly oblique/perpendicular (−40°) to the trend of the Taupō rift. The Whakatane graben is structurally complex and hosts oblique rifting (Lamarche et al., 2006) which has been shown to feature NE-SW oriented strike-slip faulting (Richardson, 1989). It is also the region where the Taupō rift intersects with the North Island dextral shear belt (Figure 7a), which is thought to induce a significant amount of dextral slip in the Whakatane graben (Lamarche et al., 2006; Mouslopoulou et al., 2007, 2008). Anisotropic fast orientations in dextral fault systems have been shown to be highly oblique to the fault strike, aligning with SH_{max} (Boness & Zoback, 2006). Therefore, it may be that the stress field in the offshore Whakatane graben is characteristic of an oblique-slip fault system.

4.3. Hikurangi Fore-Arc

For interpretations in the Hikurangi forearc, we can compare our anisotropy results to the orientation of tectonic stresses observed by Townend et al. (2012) (Figure 7a). They find that the forearc can be subdivided based on stress-orientation into two regions, northern and southern, with the transition between the two occurring near southern Hawkes Bay. In the north they find that SH_{max} is oriented NE-SW, parallel to the Hikurangi trench in a strike-slip stress regime. The NE-SW orientation of SH_{max} in this area is also observed by Warren-Smith et al. (2019), though they observe a normal faulting stress regime in the subducting plate. In contrast, in the southern forearc Townend et al. (2012) find that SH_{max} is oriented ENE-WSW, sub-parallel to the Hikurangi plate motion in a normal stress regime. The results of Townend et al. (2012) from the northern forearc contrast with our fast orientations: We observe predominantly plate-motion parallel (E-W) fast orientations in the northern forearc (Figure 9). We suggest that this is due to a sampling of different crustal depths between the two studies. Townend et al. (2012) use earthquake focal mechanisms to invert for the stress regime; thus, they are sampling the stress field at the average earthquake epicentral depth (46–68 km depth in the northern forearc). In contrast, seismic anisotropy is accrued between the earthquake epicenter and the seismometer at the surface; hence, we will be predominantly sampling the crust at shallower depths (0–40 km) than Townend et al. (2012). In the forearc, the surface of the Hikurangi slab is between 15–30 km depth (Williams et al., 2013) (Figure 10). We therefore propose that Townend et al. (2012) are measuring stress orientations within the subducting Hikurangi plate, whereas our anisotropy measurements are sampling the overlying Australian plate/forearc (Evanzia et al., 2017).

Fast orientations that are oriented NE-SW are best explained by aligned microcracks in a strike-slip stress field with SH_{max} aligned parallel to the strike of the Hikurangi slab. South of Hawkes Bay, this stress field appears to dominate in both the underlying Hikurangi slab and the overlying forearc, and this is also observed in the study of Eberhart-Phillips and Reyners (2009). The Hikurangi forearc is dominated by NE-SW aligned faults (Figure 7), and it may be that these crustal structures are also contributing to the observed NE-SW fast orientation, as observed in the central Andean margin (Reiss et al., 2018). Conversely, regions where the fast orientation is aligned E-W, for example, northern Hawkes Bay and 100–150 km along the forearc (Figure 9), may represent areas where the stress field is inducing anisotropy in the forearc and is compressional in nature. This suggests that, particularly north of Hawkes Bay, the forearc is under a compressional stress regime, whereas the underlying Hikurangi slab is undergoing strike-slip deformation. It is interesting to compare our results to a similar study from southern California (Li & Peng, 2017). Seismic anisotropy patterns from California appear to be predominantly controlled by crustal structures, such as faults. In contrast, we observe that seismic anisotropy in the Hikurangi forearc is controlled by the stress field. It may be that crustal structures in Southern California are more pervasive and/or have a more consistent alignment, at least on a local scale, than the Hikurangi forearc.

Several lines of evidence suggest the Hikurangi subduction zone exhibits different slip-behavior and forearc properties along its length. Wallace et al. (2004) show that in the southern forearc, the Hikurangi plate interface is locked with a coupling coefficient of ~1, whereas the northern forearc is not coupled and hosts frequent, shallow slow-slip events (Figure 8a) (Todd et al., 2018; Wallace et al., 2012). This low degree of plate coupling in the northern Hikurangi subduction zone may explain why we observe a significant difference between the stress fields of the Hikurangi slab and the overlying forearc there. In contrast, the strong plate-coupling in the south promotes a consistent stress field throughout. The consistent stress field in the

southern forearc was also observed by Evanzia et al. (2017), though they find variations in the stress field of the Wairarapa basin that are not observed in this study.

In addition to a change in plate coupling, marine seismic surveys and water samples show that the northern Hikurangi margin is characterized by a high fluid flux into pervasively fractured rock and mudstone (Barnes et al., 2019; Bassett et al., 2014). We have already shown that the stress field in the overlying forearc changes from south to north. Using our data, we investigate whether there is any spatial pattern in shear-wave splitting delay time (Figure 8b). We find that there is a consistent pattern, throughout the forearc, of an increase in average delay time towards the Hikurangi trench. This finding is consistent with an increase in horizontal stresses and/or an increase in the crack density towards the plate boundary. We also observe that there is a clear difference in delay-time distribution in the northern and southern forearc. Delay times measured inland are consistently higher north of Hawke's Bay than in the south, and delay times in the north increase more gradually towards the plate boundary. Our data lend support to the suggestions of Bassett et al. (2014), that high-fluid content and pervasive fractures in the northern forearc would increase the observed shear-wave splitting delay time in comparison to the southern forearc.

4.4. Subducting Hikurangi Slab

For many regions in the downgoing Hikurangi slab, the dominant fast orientation is approximately trench parallel (30°–60°) (Figure 10). This anisotropy was observed in previous shear-wave splitting studies (Audoine et al., 2004; Gledhill & Stuart, 1996; Morley et al., 2006), but, in contrast, the study of Greve and Savage (2009) proposes an isotropic slab. The observed trench-parallel fast orientation is near perpendicular to the SH_{max} orientation obtained by Townend et al. (2012), and thus we cannot explain our anisotropy results with the stress field. Seward et al. (2009) and Eberhart-Phillips and Reyners (2009) observe strong trench-parallel P-wave anisotropy within the subducting slab, with Eberhart-Phillips and Reyners (2009) observing this to depths of at least 185 km. They suggest that this anisotropic fabric is imprinted into the plate in the shallow subduction zone, where plate-bending stresses induce trench-parallel faulting (Craig et al., 2014). This observation has also been made in the Nazca subduction zone, Peru (Eakin et al., 2016), and global observations of trench-parallel teleseismic anisotropy are thought to be caused by plate-bending related faults (Faccenda et al., 2008). This hypothesis can also explain our observations of trench-parallel shear-wave splitting in the downgoing slab. However, our large catalog of measurements reveals that anisotropy is not consistently oriented through the entire subducting plate. In particular, anisotropy from earthquakes at ~120–200 km depth beneath the central North Island (Figure 10, profiles c, d, and e), shows a N-S to NW-SE fast orientation. If we continue with the hypothesis that anisotropy in the subducting slab is induced by trench-parallel structures that are formed in the shallow subduction zone, then we must consider the complex Hikurangi subduction history. While the E-W convergence direction has remained relatively constant over the last ~25 Ma, the orientation of the trench has varied (Schellart et al., 2006; Seebeck et al., 2014) and the Kermadec arc to the north underwent major reorganization as recently as 4.4 Ma (Timm et al., 2019). It may be that the differing fast orientations we see at great depths are caused by slab-bending structures formed when the subduction zone was oriented differently to the present day.

5. Conclusions

We have compiled the largest database of crustal seismic anisotropy measurements in New Zealand's North Island utilizing permanent and temporary seismic deployments. This has enabled us to map the distribution and orientation of stress and structures within the overlying Australian plate and subducting Pacific plate (specifically the Hikurangi Plateau) in great detail. We have found that

1. The majority of anisotropy in the Taranaki region is controlled by NW-SE oriented extension in the region. Fast orientations proximal to the Taranaki volcanic edifice aligns with the Taranaki lineament, suggesting that there is a lower-crustal structural control on the distribution of Taranaki volcanism.
2. At Okataina and Taupō volcanoes, the lack of a consistent fast orientation suggests the presence of large magma reservoirs beneath these two volcanoes.
3. In the central TVZ, between Okataina and Taupō, anisotropy throughout the seismogenic crust is controlled by the regional extension. This suggests that this area does not presently host magma reservoirs in the middle to the upper crust that are of comparable size to Taupō or Okataina.
4. Fast orientations in the northern TVZ are highly oblique to both the rift and the regional faults, potentially indicating that the area is characterized by an oblique-slip stress field.

5. The southern Hikurangi forearc (south of Hawke's Bay) is characterized by a strike-slip stress field with SH_{max} oriented sub-parallel to the strike of the subduction zone. Comparison to previous studies suggests that the stress field is continuous in its orientation throughout the slab and forearc in this region.
6. The northern Hikurangi forearc has anisotropic properties which suggest an E-W compressional stress regime, parallel to the direction of subduction. This reveals that in this region the stress regime in the forearc is different to that in the subducting slab. This is inferred to be a consequence of the low degree of plate coupling on the subduction interface. The northern Hikurangi forearc also has consistently higher shear-wave splitting delay times than its southern counterpart, suggesting pervasive fracturing of the forearc in this region.
7. The subducting Hikurangi slab has a predominant trench-parallel fast orientation, potentially caused by plate-bending faulting in the shallow subduction system. Changes to an oblique fast orientation at depth may be a relic of past subduction configurations.

Acknowledgments
FIK, MKS, and CJNW are funded by the ECLIPSE Programme, which is funded by the New Zealand Ministry of Business, Innovation and Employment. We thank Cynthia Ebinger for providing access to the BARNZ data, supported by the Marshall-Heape endowment at Tulane University. We also thank Geoff Lerner for fruitful discussions regarding Taranaki volcanism and two anonymous reviewers and editor Maureen Long who provided useful and insightful suggestions for the improvement of the manuscript. Waveforms were downloaded with the ObsPy package (Beyreuther et al., 2010). All figures were made using GMT (Wessel et al., 2013) and color maps from Crameri (2018). The MFAST package is available for download at http://mfast-package.geo.vuw.ac.nz. The TESSA package is available for download at https://sites.google.com/site/jessicahelenjohnson/tessa. The seismic anisotropy results are available in the supporting information and can be found with the following DOI: 10.5281/zenodo.3385288. The GeoNet seismic data is freely available from the GeoNet servers (www.geonet.org.nz); all other data can be found at the Incorporated Research Institutions for Seismology Data Management Center (IRIS-DMC) (www.ds.iris.edu/SeismiQuery).

References

Ando, M., & Ishikawa, Y. (1982). Observations of shear-wave velocity polarization anisotropy beneath Honshu, Japan. *Journal of Physics of the Earth*, *30*, 191–199.

Araragi, K. R., Savage, M. K., Ohminato, T., & Aoki, Y. (2015). Seismic anisotropy of the upper crust around Mount Fuji, Japan. *Journal of Geophysical Research: Solid Earth*, *120*, 2739–2751. https://doi.org/10.1002/2014jb011554

Audoine, E., Savage, M. K., & Gledhill, K. (2004). Anisotropic structure under a back arc spreading region, the Taupo Volcanic Zone, New Zealand. *Journal of Geophysical Research*, *109*, B11305. https://doi.org/10.1029/2003JB002932

Bannister, S. (2009). Deep Geothermal "Hotter and Deeper" seismic array International Federation of Digital Seismograph Networks. Dataset/Seismic Network.

Barker, S. J., Wilson, C. J. N., Allan, A. S. R., & Schipper, C. I. (2015). Fine-scale temporal recovery, reconstruction and evolution of a post-supereruption magmatic system. *Contributions to Mineralogy and Petrology*, *170*(1), 5.

Barnes, J. D., Cullen, J., Barker, S., Agostini, S., Penniston-Dorland, S., Lassiter, J. C., et al. (2019). The role of the upper plate in controlling fluid-mobile element (Cl, Li, B) cycling through subduction zones: Hikurangi forearc, New Zealand. *Geosphere*, *15*(3), 642–658.

Bassett, D., Sutherland, R., & Henrys, S. (2014). Slow wavespeeds and fluid overpressure in a region of shallow geodetic locking and slow slip, Hikurangi subduction margin, New Zealand. *Earth and Planetary Science Letters*, *389*, 1–13.

Bastow, I., Pilidou, S., Kendall, J.-M., & Stuart, G. (2010). Melt-induced seismic anisotropy and magma assisted rifting in Ethiopia: Evidence from surface waves. *Geochemistry, Geophysics, Geosystems*, *11*, Q0AB05. https://doi.org/10.1029/2010gc003036

Bertrand, E. A., Caldwell, T. G., Hill, G. J., Wallin, E. L., Bennie, S. L., Cozens, N., et al. (2012). Magnetotelluric imaging of upper-crustal convection plumes beneath the Taupo Volcanic Zone, New Zealand. *Geophysical Research Letters*, *39*, L02304. https://doi.org/10.1029/2011gl050177

Beyreuther, M., Barsch, R., Krischer, L., Megies, T., Behr, Y., & Wassermann, J. (2010). ObsPy: A Python toolbox for seismology. *Seismological Research Letters*, *81*(3), 530–533.

Bibby, H. M., Caldwell, T. G., Davey, F. J., & Webb, T. H. (1995). Geophysical evidence on the structure of the Taupo Volcanic Zone and its hydrothermal circulation. *Journal of Volcanology and Geothermal Research*, *68*(1-3), 29–58.

Boness, N. L., & Zoback, M. D. (2006). Mapping stress and structurally controlled crustal shear velocity anisotropy in California. *Geology*, *34*(10), 825–828.

Chambefort, I., Lewis, B., Wilson, C. J. N., Rae, A. J., Coutts, C., Bignall, G., & Ireland, T. R. (2014). Stratigraphy and structure of the Ngatamariki geothermal system from new zircon U–Pb geochronology: Implications for Taupo volcanic zone evolution. *Journal of Volcanology and Geothermal Research*, *274*, 51–70.

Cole, J. W. (1990). Structural control and origin of volcanism in the Taupo volcanic zone, New Zealand. *Bulletin of Volcanology*, *52*(6), 445–459.

Cole, J. W., Deering, C. D., Burt, R. M., Sewell, S., Shane, P. A. R., & Matthews, N. E. (2014). Okataina Volcanic Centre, Taupo volcanic zone, New Zealand: A review of volcanism and synchronous pluton development in an active, dominantly silicic caldera system. *Earth-Science Reviews*, *128*, 1–17.

Craig, T. J., Copley, A., & Jackson, J. (2014). A reassessment of outer-rise seismicity and its implications for the mechanics of oceanic lithosphere. *Geophysical Journal International*, *197*(1), 63–89.

Crameri, F. (2018). Geodynamic diagnostics, scientific visualisation and StagLab 3.0. *Geoscientific Model Development*, *11*(6), 2541–2562.

Crampin, S. (1984). An introduction to wave propagation in anisotropic media. *Geophysical Journal International*, *76*(1), 17–28.

Crampin, S. (1987). Geological and industrial implications of extensive-dilatancy anisotropy. *Nature*, *328*(6130), 491–496.

Crampin, S. (1994). The fracture criticality of crustal rocks. *Geophysical Journal International*, *118*, 428–438.

Crampin, S. (1999). Calculable fluid–rock interactions. *Geological Society, London*, *156*(3), 501–514.

Crampin, S., & Peacock, S. (2008). A review of the current understanding of seismic shear-wave splitting in the Earth's crust and common fallacies in interpretation. *Wave Motion*, *45*(6), 675–722.

Crampin, S., & Zatsepin, S. V. (1997). Modelling the compliance of crustal rock. Response to temporal changes before earthquakes. *Geophysical Journal International*, *129*(3), 495–506.

Davy, B. W., & Caldwell, T. G. (1998). Gravity, magnetic and seismic surveys of the caldera complex, Lake Taupo, North Island, New Zealand. *Journal of Volcanology and Geothermal Research*, *81*(1-2), 69–89.

Davy, B. W., & Wood, R. (1994). Gravity and magnetic modelling of the Hikurangi Plateau. *Marine Geology*, *118*(1-2), 139–151.

DeMets, C., Gordon, R. G., & Argus, D. F. (2010). Geologically current plate motions. *Geophysical Journal International*, *181*(1), 1–80.

Dimech, J.-L., Stern, T., & Lamb, S. (2017). Mantle earthquakes, crustal structure, and gravitational instability beneath western North Island, New Zealand. *Geology*, *45*(2), 155–158.

Druce, A. P. (1966). Tree-ring dating of recent volcanic ash and lapilli, Mt Egmont. *New Zealand Journal of Botany*, *4*(1), 3–41.

Dunn, R. A., Lekić, V., Detrick, R. S., & Toomey, D. R. (2005). Three-dimensional seismic structure of the Mid-Atlantic Ridge (35 N): Evidence for focused melt supply and lower crustal dike injection. *Journal of Geophysical Research*, *110*, B09101. https://doi.org/10.1029/2004jb003473

Eakin, C. M., Long, M. D., Scire, A., Beck, S. L., Wagner, L. S., Zandt, G., & Tavera, H. (2016). Internal deformation of the subducted Nazca slab inferred from seismic anisotropy. *Nature Geoscience*, *9*(1), 56–59.

Eastwood, A. A., Gravley, D. M., Wilson, C. J. N., Chambefort, I., Oze, C., Cole, J. W., & Ireland, T. R. (2013). U-Pb dating of subsurface pyroclastic deposits (Tahorakuri Formation) at Ngatamariki and Rotokawa geothermal fields. In *Proceedings of the 35th New Zealand Geothermal Workshop*, Rotorua, New Zealand.

Eberhart-Phillips, D., & Reyners, M. (2009). Three-dimensional distribution of seismic anisotropy in the Hikurangi subduction zone beneath the central North Island, New Zealand. *Journal of Geophysical Research*, *114*, B06301. https://doi.org/10.1029/2008JB005947

Eberhart-Phillips, D., Reyners, M., Faccenda, M., & Naliboff, J. (2013). Along-strike variation in subducting plate seismicity and mantle wedge attenuation related to fluid release beneath the North Island, New Zealand. *Physics of the Earth and Planetary Interiors*, *225*, 12–27.

Ebinger, C. J. (2017). Back-arc rifting in New Zealand. International Federation of Digital Seismograph Networks Dataset/Seismic Network. 10.7914/SN/YA_2017.

Ellis, S. M., Heise, W., Kissling, W., Villamor, P., & Schreurs, G. (2014). The effect of crustal melt on rift dynamics: Case study of the Taupo volcanic zone. *New Zealand Journal of Geology and Geophysics*, *57*(4), 453–458.

Ellis, S. M., Wilson, C. J. N., Bannister, S., Bibby, H. M., Heise, W., Wallace, L., & Patterson, N. (2007). A future magma inflation event under the rhyolitic Taupo volcano, New Zealand: Numerical models based on constraints from geochemical, geological, and geophysical data. *Journal of Volcanology and Geothermal Research*, *168*, 1–27.

Evanzia, D., Wilson, T., Savage, M. K., Lamb, S. L., & Hirschberg, H. (2017). Stress orientations in a locked subduction zone at the southern Hikurangi margin, New Zealand. *Journal of Geophysical Research: Solid Earth*, *122*, 7895–7911. https://doi.org/10.1002/2017JB013998

Faccenda, M., Burlini, L., Gerya, T. V., & Mainprice, D. (2008). Fault-induced seismic anisotropy by hydration in subducting oceanic plates. *Nature*, *455*(7216), 1097–1100.

Gerst, A., & Savage, M. K. (2004). Seismic anisotropy beneath Ruapehu volcano: A possible eruption forecasting tool. *Science*, *306*(5701), 1543–1547.

Giba, M., Nicol, A., & Walsh, J. J. (2010). Evolution of faulting and volcanism in a back-arc basin and its implications for subduction processes. *Tectonics*, *29*, TC4020. https://doi.org/10.1029/2009TC002634

Gledhill, K., & Stuart, G. (1996). Seismic anisotropy in the fore-arc region of the Hikurangi subduction zone, New Zealand. *Physics of the Earth and Planetary Interiors*, *95*(3-4), 211–225.

Greve, S. M., & Savage, M. K. (2009). Modelling seismic anisotropy variations across the Hikurangi subduction margin, New Zealand. *Earth and Planetary Science Letters*, *285*(1-2), 16–26.

Heise, W., Caldwell, T. G., Bibby, H. M., & Bennie, S. L. (2010). Three-dimensional electrical resistivity image of magma beneath an active continental rift, Taupo Volcanic Zone, New Zealand. *Geophysical Research Letters*, *37*, L10301. https://doi.org/10.1029/2010GL043110

Hudson, J. A. (1981). Wave speeds and attenuation of elastic waves in material containing cracks. *Geophysical Journal International*, *64*(1), 133–150.

Illsley-Kemp, F., Greenfield, T., & Keir, D. (2018). Seismic anisotropy reveals a dynamic link between adjacent magmatic segments prior to dyke intrusion. *Journal of Geophysical Research: Solid Earth*, *123*, 9800–9816. https://doi.org/10.1029/2018JB016420

Illsley-Kemp, F., Savage, M. K., Keir, D., Hirschberg, H. P., Bull, J. M., Gernon, T. M., et al. (2017). Extension and stress during continental breakup: Seismic anisotropy of the crust in Northern Afar. *Earth and Planetary Science Letters*, *477*, 41–51.

Johnson, J. H., & Savage, M. K. (2012). Tracking volcanic and geothermal activity in the Tongariro Volcanic Centre, New Zealand, with shear wave splitting tomography. *Journal of Volcanology and Geothermal Research*, *223*, 1–10.

Johnson, J. H., Savage, M. K., & Townend, J. (2011). Distinguishing between stress-induced and structural anisotropy at Mount Ruapehu Volcano, New Zealand. *Journal of Geophysical Research*, *116*, B12303. https://doi.org/10.1029/2011JB008308

Keir, D., Belachew, M., Ebinger, C. J., Kendall, J.-M., Hammond, J. O. S., Stuart, G. W., et al. (2011). Mapping the evolving strain field during continental breakup from crustal anisotropy in the Afar Depression. *Nature Communications*, *2*, 285.

King, P. R. (2000). Tectonic reconstructions of New Zealand: 40 Ma to the present. *New Zealand Journal of Geology and Geophysics*, *43*(4), 611–638.

Lamarche, G., Barnes, P. M., & Bull, J. M. (2006). Faulting and extension rate over the last 20,000 years in the offshore Whakatane Graben, New Zealand continental shelf. *Tectonics*, *25*, TC4005. https://doi.org/10.1029/2005TC001886

Li, Z., & Peng, Z. (2017). Stress and structure induced anisotropy in southern California from two decades of shear wave splitting measurements. *Geophysical Research Letters*, *44*, 9607–9614. https://doi.org/10.1002/2017GL075163

Li, Z., Zhang, H., & Peng, Z. (2014). Structure-controlled seismic anisotropy along the Karadere–Düzce branch of the North Anatolian Fault revealed by shear-wave splitting tomography. *Earth and Planetary Science Letters*, *391*, 319–326.

Little, T. A., Van Dissen, R., Rieser, U., Smith, E. G., & Langridge, R. M. (2010). Coseismic strike slip at a point during the last four earthquakes on the Wellington fault near Wellington, New Zealand. *Journal of Geophysical Research*, *115*, B05403. https://doi.org/10.1029/2009JB006589

Liu, Y., Anderson, A. T., Wilson, C. J. N., Davis, A. M., & Steele, I. M. (2006). Mixing and differentiation in the Oruanui rhyolitic magma, Taupo, New Zealand: Evidence from volatiles and trace elements in melt inclusions. *Contributions to Mineralogy and Petrology*, *151*(1), 71–87.

Maher, S., & Kendall, J.-M. (2018). Crustal anisotropy and state of stress at Uturuncu Volcano, Bolivia, from shear-wave splitting measurements and magnitude–frequency distributions in seismicity. *Earth and Planetary Science Letters*, *495*, 38–49.

Mazzarini, F., Le Corvec, N., Isola, I., & Favalli, M. (2016). Volcanic field elongation, vent distribution, and tectonic evolution of a continental rift: The Main Ethiopian Rift example. *Geosphere*, *12*(3), 706–720.

Morley, A. M., Stuart, G. W., Kendall, J.-M., & Reyners, M. (2006). Mantle wedge anisotropy in the Hikurangi subduction zone, central North Island, New Zealand. *Geophysical Research Letters*, *33*, L05301. https://doi.org/10.1029/2005GL024569

Mortimer, N., & Parkinson, D. (1996). Hikurangi Plateau: A Cretaceous large igneous province in the southwest Pacific Ocean. *Journal of Geophysical Research*, *101*, 687–696. https://doi.org/10.1029/95JB03037

Mouslopoulou, V., Nicol, A., Little, T., & Walsh, J. (2007). Displacement transfer between intersecting regional strike-slip and extensional fault systems. *Journal of Structural Geology*, *29*(1), 100–116.

Mouslopoulou, V., Nicol, A., Walsh, J., Beetham, D., & Stagpoole, V. (2008). Quaternary temporal stability of a regional strike-slip and rift fault intersection. *Journal of Structural Geology*, *30*(4), 451–463.

Mroczek, S., Savage, M. K., Hopp, C., & Sewell, S. M. (2019). Anisotropy as an indicator for reservoir changes: Example from the Rotokawa and Ngatamariki geothermal fields, New Zealand. *Geophysical Journal International*, *220*91), 1–17. https://doi.org/10.1093/gji/ggz400

Neall, V. E., Smith, I. E. M., & Stewart, R. B. (1986). History and petrology of the Taranaki volcanoes, *Late Cenozoic Volcanism in New Zealand, Roy. Soc. N. Z. Bull.* (Vol. 23, pp. 251–263). Wellington: Royal Society of New Zealand.

Nicol, A., Mazengarb, C., Chanier, F., Rait, G., Uruski, C., & Wallace, L. (2007). Tectonic evolution of the active Hikurangi subduction margin, New Zealand, since the Oligocene. *Tectonics*, *26*, TC4002. https://doi.org/10.1029/2006TC002090

Petersen, T., Gledhill, K., Chadwick, M., Gale, N. H., & Ristau, J. (2011). The New Zealand national seismograph network. *Seismological Research Letters*, *82*(1), 9–20.

Price, R. C., Stewart, R. B., Woodhead, J. D., & Smith, I. E. M. (1999). Petrogenesis of high-K arc magmas: Evidence from Egmont volcano, North Island, New Zealand. *Journal of Petroleum*, *40*(1), 167–197.

Reiss, M. C., Rümpker, G., & Wölbern, I. (2018). Large-scale trench-normal mantle flow beneath central South America. *Earth and Planetary Science Letters*, *482*, 115–125.

Reyners, M. (1998). Plate coupling and the hazard of large subduction thrust earthquakes at the Hikurangi subduction zone, New Zealand. *New Zealand Journal of Geology and Geophysics*, *41*(4), 343–354.

Reyners, M., Eberhart-Phillips, D., & Bannister, S. (2011). Tracking repeated subduction of the Hikurangi Plateau beneath New Zealand. *Earth and Planetary Science Letters*, *311*(1-2), 165–171.

Reyners, M., & Stuart, G. (2002). The central North Island passive seismic experiment (Science Report 2001–011): Institute of Geological & Nuclear Sciences.

Richardson, W. P. (1989). The Matata earthquake of 1977 May 31: A recent event near Edgecumbe, Bay of Plenty, New Zealand. *New Zealand Journal of Geology and Geophysics*, *32*(1), 17–30.

Rodgers, D. W., & Little, T. A. (2006). World's largest coseismic strike-slip offset: The 1855 rupture of the Wairarapa Fault, New Zealand, and implications for displacement/length scaling of continental earthquakes. *Journal of Geophysical Research*, *111*, B12408. https://doi.org/10.1029/2005JB004065

Rowland, J. V., & Sibson, R. H. (2001). Extensional fault kinematics within the Taupo Volcanic Zone, New Zealand: Soft-linked segmentation of a continental rift system. *New Zealand Journal of Geology and Geophysics*, *44*(2), 271–283.

Salmon, M. L., Stern, T. A., & Savage, M. K. (2011). A major step in the continental Moho and its geodynamic consequences: The Taranaki-Ruapehu line, New Zealand. *Geophysical Journal International*, *186*(1), 32–44.

Savage, M. K. (1999). Seismic anisotropy and mantle deformation: What have we learned from shear wave splitting? *Reviews of Geophysics*, *37*(1), 65–106.

Savage, M., Ferrazzini, V., Peltier, A., Rivemale, E., Mayor, J., Schmid, A., et al. (2015). Seismic anisotropy and its precursory change before eruptions at Piton de la Fournaise volcano, La Réunion. *Journal of Geophysical Research: Solid Earth*, *120*, 3430–3458. https://doi.org/10.1002/2014JB011665

Savage, M. K., Wessel, A., Teanby, N. A., & Hurst, A. W. (2010). Automatic measurement of shear wave splitting and applications to time varying anisotropy at Mount Ruapehu volcano, New Zealand. *Journal of Geophysical Research*, *115*, B12321. https://doi.org/10.1029/2010JB007722

Schellart, W. P., Lister, G. S., & Toy, V. G. (2006). A Late Cretaceous and Cenozoic reconstruction of the Southwest Pacific region: Tectonics controlled by subduction and slab rollback processes. *Earth-Science Reviews*, *76*(3-4), 191–233.

Seebeck, H., Nicol, A., Giba, M., Pettinga, J., & Walsh, J. (2014). Geometry of the subducting Pacific plate since 20 Ma, Hikurangi margin, New Zealand. *Journal of the Geological Society, London*, *171*(1), 131–143.

Seebeck, H., Nicol, A., Stern, T. A., Bibby, H. M., & Stagpoole, V. (2010). Fault controls on the geometry and location of the Okataina Caldera, Taupo Volcanic Zone, New Zealand. *Journal of Volcanology and Geothermal Research*, *190*(1-2), 136–151.

Seebeck, H., Nicol, A., Villamor, P., Ristau, J., & Pettinga, J. (2014). Structure and kinematics of the Taupo Rift, New Zealand. *Tectonics*, *33*, 1178–1199. https://doi.org/10.1002/2014TC003569

Self, S., Goff, F., Gardner, J. N., Wright, J. V., & Kite, W. M. (1986). Explosive rhyolitic volcanism in the Jemez Mountains: Vent locations, caldera development and relation to regional structure. *Journal of Geophysical Research*, *91*, 1779–1798. https://doi.org/10.1029/jb091ib02p01779

Seward, A. M., Henderson, C. M., & Smith, E. G. C. (2009). Models of the upper mantle beneath the central North Island, New Zealand, from speeds and anisotropy of subhorizontal P waves (Pn). *Journal of Geophysical Research*, *114*, B01301. https://doi.org/10.1029/2008JB005805

Shaddox, H. R., & Schwartz, S. Y. (2019). Subducted seamount diverts shallow slow slip to the forearc of the northern Hikurangi subduction zone, New Zealand. *Geology*, *47*(5), 415–418.

Sherburn, S., & White, R. S. (2006). Tectonics of the Taranaki region, New Zealand: Earthquake focal mechanisms and stress axes. *New Zealand Journal of Geology and Geophysics*, *49*(2), 269–279.

Silver, P. G., & Chan, W. W. (1991). Shear wave splitting and subcontinental mantle deformation. *Journal of Geophysical Research*, *96*, 16,429–16,454. https://doi.org/10.1029/91JB00899

Smith, E. G. C., Stern, T. A., & Reyners, M. (1989). Subduction and back-arc activity at the Hikurangi convergent margin, New Zealand. *Pure and Applied Geophysics*, *129*(1-2), 203–231.

Stagpoole, V., & Nicol, A. (2008). Regional structure and kinematic history of a large subduction back thrust: Taranaki Fault, New Zealand. *Journal of Geophysical Research*, *113*, B01403. https://doi.org/10.1029/2007JB005170

Stern, T. A., & Benson, A. (2011). Wide-angle seismic imaging beneath an andesitic arc: Central North Island, New Zealand. *Journal of Geophysical Research*, *116*, B09308. https://doi.org/10.1029/2011JB008337

Stern, T. A., Houseman, G., Salmon, M., & Evans, L. (2013). Instability of a lithospheric step beneath western North Island, New Zealand. *Geology*, *41*(4), 423–426.

Taylor, B. (2006). The single largest oceanic plateau: Ontong Java–Manihiki–Hikurangi. *Earth and Planetary Science Letters*, *241*(3-4), 372–380.

Teanby, N. A., Kendall, J.-M., & van der Baan, M. (2004). Automation of shear-wave splitting measurements using cluster analysis. *Bulletin of the Seismological Society of America*, *94*(2), 453–463.

Timm, C., de Ronde, C. E. J., Hoernle, K., Cousens, B., Wartho, J.-A., Tontini, F. C., et al. (2019). New age and geochemical data from the Southern Colville and Kermadec Ridges, SW Pacific: Insights into the recent geological history and petrogenesis of the proto-Kermadec (Vitiaz) Arc. *Gondwana Research*, *72*, 169–193.

Todd, E. K., Schwartz, S. Y., Mochizuki, K., Wallace, L. M., Sheehan, A. F., Webb, S. C., et al. (2018). Earthquakes and tremor linked to seamount subduction during shallow slow slip at the Hikurangi Margin, New Zealand. *Journal of Geophysical Research: Solid Earth*, *123*(8), 6769–6783.

Townend, J., Sherburn, S., Arnold, R., Boese, C., & Woods, L. (2012). Three-dimensional variations in present-day tectonic stress along the Australia–Pacific plate boundary in New Zealand. *Earth and Planetary Science Letters*, *353–354*, 47–59.

Tozer, B., Stern, T. A., Lamb, S. L., & Henrys, S. A. (2017). Crust and upper-mantle structure of Wanganui Basin and southern Hikurangi margin, North Island, New Zealand as revealed by active source seismic data. *Geophysical Journal International*, *211*(2), 718–740.

Van Dissen, R. J., & Berryman, K. R. (1996). Surface rupture earthquakes over the last ~1000 years in the Wellington region, New Zealand, and implications for ground shaking hazard. *Journal of Geophysical Research*, *101*, 5999–6019.

Villamor, P., & Berryman, K. R. (2001). A late Quaternary extension rate in the Taupo Volcanic Zone, New Zealand, derived from fault slip data. *New Zealand Journal of Geology and Geophysics*, *44*(2), 243–269.

Villamor, P., & Berryman, K. R. (2006a). Evolution of the southern termination of the Taupo Rift, New Zealand. *New Zealand Journal of Geology and Geophysics*, *49*(1), 23–37.

Villamor, P., & Berryman, K. R. (2006b). Late Quaternary geometry and kinematics of faults at the southern termination of the Taupo Volcanic Zone, New Zealand. *New Zealand Journal of Geology and Geophysics*, *49*(1), 1–21.

Wadge, G., Biggs, J., Lloyd, R., & Kendall, J.-M. (2016). Historical volcanism and the state of stress in the East African Rift System. *Frontiers in Earth Science*, *4*, 86.

Wallace, L. M., Beavan, J., Bannister, S., & Williams, C. (2012). Simultaneous long-term and short-term slow slip events at the Hikurangi subduction margin, New Zealand: Implications for processes that control slow slip event occurrence, duration, and migration. *Journal of Geophysical Research*, *117*, B11402. https://doi.org/10.1029/2012jb009489

Wallace, L. M., Beavan, J., McCaffrey, R., & Darby, D. (2004). Subduction zone coupling and tectonic block rotations in the North Island, New Zealand. *Journal of Geophysical Research*, *109*, B1240. https://doi.org/10.1029/2004JB003241

Warren-Smith, E., Fry, B., Wallace, L., Chon, E., Henrys, S., Sheehan, A., et al. (2019). Episodic stress and fluid pressure cycling in subducting oceanic crust during slow slip. *Nature Geoscience*, *12*, 475–481.

Wessel, P., Smith, W. H., Scharroo, R., Luis, J., & Wobbe, F. (2013). Generic mapping tools: Improved version released. *Eos Transactions American Geophysical Union*, *94*(45), 409–410.

Wiart, P., & Oppenheimer, C. (2005). Large magnitude silicic volcanism in north Afar: The Nabro Volcanic Range and Maalalta volcano. *Bulletin of Volcanology*, *67*(2), 99–115.

Williams, C. A., Eberhart-Phillips, D., Bannister, S., Barker, D. H., Henrys, S., Reyners, M., & Sutherland, R. (2013). Revised interface geometry for the Hikurangi subduction zone, New Zealand. *Seismological Research Letters*, *84*(6), 1066–1073.

Wilson, C. J. N., Gravley, D. M., Leonard, G. S., & Rowland, J. V. (2009). Volcanism in the central Taupo volcanic zone, New Zealand: tempo, styles and controls. *Studies in Volcanology: The Legacy of George Walker. Special Publications of IAVCEI*, *2*, 225–247.

Wilson, C. J. N., Houghton, B. F., McWilliams, M. O., Lanphere, M. A., Weaver, S. D., & Briggs, R. M. (1995). Volcanic and structural evolution of Taupo Volcanic Zone, New Zealand: A review. *Journal of Volcanology and Geothermal Research*, *68*(1-3), 1–28.

Wood, R., & Davy, B. (1994). The Hikurangi Plateau. *Marine Geology*, *118*(1-2), 153–173.

Zernack, A. V., Price, R. C., Smith, I. E. M., Cronin, S. J., & Stewart, R. B. (2011). Temporal evolution of a high-K andesitic magmatic system: Taranaki volcano, New Zealand. *Journal of Petrology*, *53*(2), 325–363.

Zinke, J. C., & Zoback, M. D. (2000). Structure-related and stress-induced shear-wave velocity anisotropy: Observations from microearthquakes near the Calaveras Fault in Central California. *Bulletin of the Seismological Society of America*, *90*, 1305–1312.